


Effect of a Chern-Simons term on dynamical gap generation in graphene

M. E. Carrington*

*Department of Physics, Brandon University, Brandon, Manitoba, Canada R7A 6A9
and Winnipeg Institute for Theoretical Physics, Winnipeg, Manitoba, Canada*

 (Received 20 December 2018; revised manuscript received 21 February 2019; published 25 March 2019)

We study the effect of a Chern-Simons term on dynamical gap generation in a low-energy effective theory that describes some features of monolayer suspended graphene. We use a nonperturbative Schwinger-Dyson approach. We solve a set of coupled integral equations for eight independent dressing functions that describe fermion and photon degrees of freedom. We find a strong suppression of the gap and corresponding increase in the critical coupling as a function of increasing Chern-Simons coefficient.

DOI: [10.1103/PhysRevB.99.115432](https://doi.org/10.1103/PhysRevB.99.115432)

I. INTRODUCTION

Quantum electrodynamics in 2+1 dimensions (QED_{2+1}) has been studied for many years as a toy model for quantum chromodynamics (QCD). The main point is that QED_{2+1} is strongly coupled, and therefore, in spite of being Abelian, it can be used to study many interesting features of QCD [1–5]. In this paper, we are interested in reduced QED_{3+1} (RQED) in which the fermions are restricted to remain in a two-dimensional plane but the photons which are responsible for the interactions between fermions are not. In the reduced theory the Coulomb interaction between the electrons has the same $1/r$ form as in the (3+1)-dimensional theory, instead of the logarithmic form obtained from QED_{2+1} . The theory is physically relevant for the description of what are called Dirac planar materials, which refer to condensed-matter systems for which the underlying lattice structure produces a fermionic dispersion relation that has the form of a Dirac equation in some regimes. We are particularly interested in graphene, where the fermions have an effective speed v_F which is on the order of 300 times smaller than the speed of light. The unique band structure of graphene gives it high mobility, large thermal and electrical conductivity, and optical transparency, which are characteristics that are valuable in technological applications. We study specifically suspended single-layer graphene, where we deal with a single atomic layer in the absence of scattering from a substrate, so that the intrinsic electronic properties of the system are accessed. For simplicity we will also work at half filling (which means zero chemical potential).

In both QED_{2+1} and RQED the fermions couple to a three-dimensional Abelian gauge field, and therefore, the Chern-Simons (CS) term can be added to the action. This term breaks the time-reversal symmetry and gives a mass to the photon. It is important in condensed-matter physics in the context of chiral symmetry breaking [6–9], high-temperature superconductivity [10], and the Hall effect [11]. CS terms can dynamically generate magnetic fields in QED_{2+1} [12], and

magnetic fields are thought to influence dynamical symmetry breaking in a universal and model-independent way through what is known as magnetic catalysis (for a review see [13]).

In this work we use RQED and study the influence of a CS term on phase transitions in graphene. We will show in Sec. II B that the CS term has the same properties under discrete symmetry transformations as a chirally symmetric mass term which was discussed in the context of graphene by Haldane [14]. One therefore expects that including a CS term in the photon part of the action could dynamically generate a Haldane-type mass for the fermions. In Appendix B we show that such a mass term in the Lagrangian of the effective theory would correspond physically to including in the Hamiltonian of the discrete theory a contribution that would give counterclockwise hopping around the triangles that are formed by each sublattice of the graphene sheet. In [14] it was originally proposed that such hopping could take place in response to an externally applied magnetic field, and as mentioned above, the influence of magnetic fields on the phase transition in graphene is a subject of much interest. Within an effective theory description, a natural way to investigate this is through the introduction of a CS term at the level of the Lagrangian.

The coupling constant and CS parameter are dimensionful scales in QED_{2+1} , but they are dimensionless parameters in RQED. In natural units the effective coupling can be written $\alpha = e^2/(4\pi\epsilon v_F)$, where $v_F \sim c/300$ is the velocity of a massless electron in graphene. The parameter $\epsilon \geq 1$ is related to the screening properties of the graphene sheet, and we take the vacuum value $\epsilon = 1$. The Chern-Simons parameter will be denoted θ , and we consider $\theta \in (0, 1)$.

II. THE LOW-ENERGY EFFECTIVE THEORY

A. Noninteracting Hamiltonian

The carbon atoms in graphene are arranged in a two-dimensional hexagonal lattice. The hexagonal structure can be viewed as two sets of interwoven triangular sublattices (called *A* and *B*). The geometry dictates each primitive cell has one atom from the *A* sublattice and one from the *B* sublattice and that each lattice site has three nearest neighbors on the

*carrington@brandonu.ca

opposite sublattice. For each atom, three of the four outer electrons form hybridized σ bonds with the three nearest neighbors. The fourth sits in the p_z orbital, perpendicular to the hybrid orbitals, and forms a π bond. The simplest description of graphene is a tight-binding Hamiltonian for the π orbitals,

$$H_0 = -t \sum_{\langle \vec{n}\vec{n}' \rangle} [a_{n\sigma}^\dagger b_{n'\sigma} + \text{H.c.}], \quad (1)$$

where t is the nearest-neighbor hopping parameter and the operators $a_{n\sigma}^\dagger$ and $b_{n'\sigma}^\dagger$ are creation operators for π electrons with spin σ on the A and B sublattices, respectively.

We can rewrite the Hamiltonian as a momentum integral by Fourier transforming. Our definitions for the lattice vectors and discrete Fourier transforms are given in Appendix A. From the dispersion relation for the noninteracting theory we obtain six K points, and our choice of two inequivalent ones, which we denote K_\pm , is given in Eq. (A5). Using Eqs. (A6) and ((A7)), we rewrite the Hamiltonian in (1) as a momentum integral, and we expand around K_\pm . We define a four-component spinor:

$$\Psi_\sigma(\vec{p}) = (a_\sigma(\vec{K}_+ + \vec{p}), b_\sigma(\vec{K}_+ + \vec{p}), b_\sigma(\vec{K}_- + \vec{p}), a_\sigma(\vec{K}_- + \vec{p}))^T, \quad (2)$$

where the superscript T indicates that the spinor should be written as a column vector. Using this notation, the tight-binding Hamiltonian becomes

$$H_0 = \hbar v_F \sum_\sigma \int \frac{d^2 p}{(2\pi)^2} \bar{\Psi}_\sigma(\vec{p}) (\gamma^1 p_1 + \gamma^2 p_2) \Psi_\sigma(\vec{p}), \quad (3)$$

where we have defined $\hbar v_F = 3at/2$ and our representation for the gamma matrices is given in Eq. (A7). The Lagrangian of the effective theory (including minimal coupling to the gauge field) then takes the form [15]

$$\mathcal{L} = \sum_\sigma \bar{\Psi}_\sigma(t, \vec{x}) [i\gamma^0 D_t + i\hbar v_F \vec{\gamma} \cdot \vec{D}] \Psi_\sigma(t, \vec{x}), \quad (4)$$

where we define $D_\mu = \partial_\mu - ieA_\mu$ (taking $e > 0$).

In the next sections we will discuss how to include interactions. At this point however, we note that while our effective theory can accurately describe the low-energy dynamics of the system and allow us to correctly include both frequency and nonperturbative effects, it does not allow for the inclusion of screening from the σ -band electrons and localized higher-energy states.

B. Symmetries

We consider the discrete symmetries of the tight-binding Hamiltonian. The parity, time-reversal, and charge-conjugation transformations on the spinor in (2) are

$$P\Psi(\vec{p})P^{-1} = \gamma^0\Psi(-\vec{p}), \quad (5)$$

$$T\Psi(\vec{p})T^{-1} = i\sigma_2\gamma^1\gamma^5\Psi(-\vec{p}), \quad (6)$$

$$C\Psi(\vec{p})C^{-1} = \gamma^1\bar{\Psi}(\vec{p})^T. \quad (7)$$

It is easy to check that the noninteracting theory is invariant under these symmetries. To see the physical content of

Eqs. (5)–(7) we show the action of each on the spinor defined in Eq. (2).

The parity transformation takes the form

$$\Psi = \begin{pmatrix} a_\sigma(K_+ + \vec{p}) \\ b_\sigma(K_+ + \vec{p}) \\ b_\sigma(K_- + \vec{p}) \\ a_\sigma(K_- + \vec{p}) \end{pmatrix} \xrightarrow{P} \begin{pmatrix} b_\sigma(K_- - \vec{p}) \\ a_\sigma(K_- - \vec{p}) \\ a_\sigma(K_+ - \vec{p}) \\ b_\sigma(K_+ - \vec{p}) \end{pmatrix}, \quad (8)$$

which tells us that the parity operator reverses the sign of the momentum and exchanges the sublattices. We note that this definition is different from the one commonly used in QED₂₊₁, where the transformation $\mathcal{P} : (x, y) \rightarrow (-x, -y)$ would correspond to spatial rotation. Because of the hexagonal lattice structure of graphene, spatial rotation is not a symmetry of the system unless the sublattice indices are interchanged.

The time-reversal operator changes the sign of momentum and spin, and its action on a spinor is

$$\Psi = \begin{pmatrix} a_\sigma(K_+ + \vec{p}) \\ b_\sigma(K_+ + \vec{p}) \\ b_\sigma(K_- + \vec{p}) \\ a_\sigma(K_- + \vec{p}) \end{pmatrix} \xrightarrow{T} \begin{pmatrix} a_\sigma(K_- - \vec{p}) \\ b_\sigma(K_- - \vec{p}) \\ b_\sigma(K_+ - \vec{p}) \\ a_\sigma(K_+ - \vec{p}) \end{pmatrix} \quad (9)$$

(where we have not explicitly written the action of the factor $i\sigma_2$, which flips spin), and therefore, the time-reversal operator inverts the K points (and spin) but does not act on the sublattice degrees of freedom.

The action of the charge-conjugation operator is

$$\Psi = \begin{pmatrix} a_\sigma(K_+ + \vec{p}) \\ b_\sigma(K_+ + \vec{p}) \\ b_\sigma(K_- + \vec{p}) \\ a_\sigma(K_- + \vec{p}) \end{pmatrix} \xrightarrow{C} \begin{pmatrix} -b_\sigma^\dagger(K_+ + \vec{p}) \\ -a_\sigma^\dagger(K_+ + \vec{p}) \\ a_\sigma^\dagger(K_- + \vec{p}) \\ b_\sigma^\dagger(K_- + \vec{p}) \end{pmatrix}. \quad (10)$$

We can also consider continuous symmetries of the low-energy effective theory. The action is invariant under the enlarged group of global symmetries generated by both γ_5 and the third spatial gamma matrix γ_3 , which is not part of the Lagrangian (4). The matrices

$$T_1 = \frac{i}{2}\gamma^3, \quad T_2 = \frac{1}{2}\gamma^5, \quad T_3 = \frac{i}{2}\gamma^3\gamma^5 \quad (11)$$

commute with the Hamiltonian. They also satisfy the commutation relations $[T^i, T^j] = i\epsilon^{ijk}T^k$ and therefore form a four-dimensional representation of $SU(2)$. Including $T_4 = \mathbb{I}/2$ gives a representation of $U(2)$. Physically this is a symmetry in the space of valley and sublattice indices, where ‘‘valley’’ refers to the K_\pm points. The noninteracting theory has a global $U(4)$ symmetry that operates in the space of [valley \otimes sublattice \otimes spin]. We call this a chiral symmetry, and using our representation of the gamma matrices (see Appendix A), the chirality quantum number corresponds to the valley index.

C. Fermion bilinears

One reason that fermion bilinears are interesting is that, close to the critical point, possible interactions of the low-energy theory are constrained to have the form of local four-fermion interactions. For example, in the Gross-Neveu model the basic interaction is a four-fermion contact between scalar or pseudoscalar densities, and in the Thirring model

TABLE I. Transformation properties of the bilinears defined in Eq. (13) under P , C , T .

	P	C	T
\mathbb{I}	+	+	+
γ^μ	$\tilde{\dagger}$	-	$\tilde{\dagger}$
γ^3	-	+	+
$i\gamma^5$	-	-	+
$i\gamma^\mu\gamma^\nu$	$\tilde{\dagger}$	-	$\tilde{-}$
$i\gamma^\mu\gamma^3$	$\tilde{-}$	+	$\tilde{-}$
$\gamma^\mu\gamma^5$	$\tilde{-}$	-	$\tilde{-}$
$\gamma^3\gamma^5$	+	+	-

the interaction is a contact between two conserved currents. We note that while short-range interactions are not relevant for dynamics in a perturbative theory, they can be important in a strongly coupled system. Mass scales are especially interesting because they are directly related to chiral symmetry breaking and a possible semimetal/insulator transition.

We use $\Gamma^{(n)}$ to indicate one element of the list,

$$\Gamma = \{\mathbb{I}, \gamma^\mu, \gamma^3, i\gamma^5, i\gamma^\mu\gamma^\nu, i\gamma^\mu\gamma^3, \gamma^\mu\gamma^5, \gamma^3\gamma^5\}, \quad (12)$$

with $\mu \in (0, 1, 2)$, which gives a complete basis in Dirac space. We define a set of fermion bilinears as

$$\mathcal{G}^{(n)} = m^{(n)} \int d^2x \bar{\Psi}(\vec{x}) \Gamma^{(n)} \Psi(\vec{x}). \quad (13)$$

The terms constructed with scalar/pseudoscalar elements $\Gamma^{(n)} \in \{\mathbb{I}, \gamma^3, i\gamma^5, \gamma^3\gamma^5\}$ correspond to mass terms and will be denoted \mathcal{M} , \mathcal{M}^3 , \mathcal{M}^5 , and \mathcal{M}^{35} .

We look at the transformation properties of fermion bilinears under parity, time reversal, and charge conjugation. We introduce the notation $\gamma^{\tilde{\mu}} = (\gamma^0, -\gamma^i)$, with $i \in (1, 2)$. Two examples where this notation can be used are $P\bar{\Psi}\gamma^\mu\Psi P^{-1} = \bar{\Psi}\gamma^{\tilde{\mu}}\Psi$ and $P\bar{\Psi}\gamma^\mu\gamma^5\Psi P^{-1} = -\bar{\Psi}\gamma^{\tilde{\mu}}\gamma^5\Psi$. Our results are

shown in Table I, and transformations of the type discussed above are listed with a tilde over the sign. The first of the two examples given above is written $\tilde{\dagger}$ in the second row of the second column of Table I, and the second is the symbol $\tilde{-}$ in the seventh row of the second column. The mass terms \mathcal{M}^3 and \mathcal{M}^5 can be accessed from the standard Dirac mass \mathcal{M} by a change of integration variables in the path integral. The mass \mathcal{M}^{35} is completely independent of the other three and is related to a model introduced by Haldane [14]. We remark that although actions constructed from an effective Lagrangian with mass term \mathcal{M} , \mathcal{M}^3 , or \mathcal{M}^5 will describe identical physics, the symmetries of a continuous theory are not necessarily evident in the original discrete theory, which means that equivalent continuous theories may correspond to different discrete theories.

To see directly how mass terms are related to physical quantities in the discrete theory, we look at a specific example. We consider a term in the Hamiltonian of the form

$$H_1 = \sum_{\vec{n}\sigma} [m_a a_{\vec{n}\sigma}^\dagger a_{\vec{n}\sigma} + m_b b_{\vec{n}\sigma}^\dagger b_{\vec{n}\sigma}], \quad (14)$$

which would correspond to different densities of particles on the A and B sublattices and could be realized physically by placing the graphene sheet on a substrate. Fourier transforming to momentum space and expanding around the K points, Eq. (14) becomes

$$H_1 = \sum_{\sigma} \int \frac{d^2p}{(2\pi)^2} [m_+ \bar{\Psi}_{\sigma}(\vec{p}) \gamma_0 \Psi_{\sigma}(\vec{p}) + m_- \bar{\Psi}_{\sigma}(\vec{p}) \gamma_3 \Psi_{\sigma}(\vec{p})], \quad (15)$$

where we have defined $m_{\pm} = \frac{1}{2}(m_a \pm m_b)$. The term in (15) with the factor m_- is proportional to the \mathcal{M}^3 mass term, which breaks parity. Writing it explicitly in terms of creation and annihilation operators, we obtain

$$\begin{aligned} \mathcal{M}^3 = \int d^2x \bar{\Psi} \gamma^3 \Psi = \sum_{\sigma} \int \frac{d^2p}{(2\pi)^2} \{ & [a_{\sigma}^\dagger(\vec{K}_+ + \vec{p}) a_{\sigma}(\vec{K}_+ + \vec{p}) + a_{\sigma}^\dagger(\vec{K}_- + \vec{p}) a_{\sigma}(\vec{K}_- + \vec{p})] \\ & - [(b_{\sigma}^\dagger(\vec{K}_+ + \vec{p}) b_{\sigma}(\vec{K}_+ + \vec{p}) + b_{\sigma}^\dagger(\vec{K}_- + \vec{p}) b_{\sigma}(\vec{K}_- + \vec{p}))], \end{aligned} \quad (16)$$

which makes clear that the order parameter \mathcal{M}^3 is proportional to the difference in electron densities for the A and B sublattices. A nonzero value of this order parameter corresponds physically to a charge density wave and lifts the sublattice degeneracy. The term in (15) that is proportional to m_+ is less interesting since it can be absorbed into a redefinition of the chemical potential.

The independent mass term

$$\begin{aligned} \mathcal{M}^{35} = \int d^2x \bar{\Psi} \gamma^3 \gamma^5 \Psi = \sum_{\sigma} \int \frac{d^2p}{(2\pi)^2} \{ & [a_{\sigma}^\dagger(\vec{K}_+ + \vec{p}) a_{\sigma}(\vec{K}_+ + \vec{p}) - a_{\sigma}^\dagger(\vec{K}_- + \vec{p}) a_{\sigma}(\vec{K}_- + \vec{p})] \\ & - [(b_{\sigma}^\dagger(\vec{K}_+ + \vec{p}) b_{\sigma}(\vec{K}_+ + \vec{p}) - b_{\sigma}^\dagger(\vec{K}_- + \vec{p}) b_{\sigma}(\vec{K}_- + \vec{p}))] \end{aligned} \quad (17)$$

corresponds to a gap with opposite sign at the K_- point, relative to \mathcal{M}^3 . Mathematically, a triangular next-neighbor hopping term in the Hamiltonian of the discrete theory gives a mass term proportional to \mathcal{M}^{35} in the effective theory. This is shown in Appendix B. Physically it corresponds to a topologically nontrivial phase generated by currents propagating on

the two different sublattices. Both the CS term and the \mathcal{M}^{35} mass term violate time-reversal invariance (see Table I), and one therefore expects that one-loop radiative corrections to the photon polarization tensor obtained from internal fermions with a Haldane-type mass would generate an odd- T piece in the polarization tensor or that including a CS term in

the photon part of the action would dynamically generate a Haldane-type mass for the fermions. In this paper we will introduce a CS term into the action and study the effect of this term through dynamical mass generation on phase transitions in graphene.

D. The brane action

Dynamical photons are included in RQED by constructing the brane action [16–18]. We start with the four-dimensional Euclidean action

$$S = \int d^4x \left[\frac{1}{4} F_{\mu\nu} F_{\mu\nu} - \frac{1}{2\xi} (\partial_\mu A_\mu)^2 + ie \bar{\Psi} \not{A} \Psi \right] \quad (18)$$

and integrate out the four-dimensional gauge field to obtain

$$S \rightarrow \frac{1}{2} \int d^4x \int d^4y J_\mu(x) D_{\mu\nu}(x-y) J_\nu(y),$$

$$D_{\mu\nu}(x-y) = \int \frac{d^3K}{(2\pi)^3} \int \frac{dk_3}{2\pi} e^{ik(x-y)} \times \left[\delta_{\mu\nu} - (1-\xi) \frac{k_\mu k_\nu}{K^2 + k_3^2} \right] \frac{1}{K^2 + k_3^2}, \quad (19)$$

where we write $k = (K, k_3)$. We use capital letters for three vectors which include a timelike component, for example, $K = (k_0, \vec{k}) = (k_0, k_1, k_2)$ and $X = (x_0, \vec{x}) = (x_0, x_1, x_2)$. To describe graphene we take

$$J_3 = 0, \quad J_\mu(x_0, x_1, x_2, x_3) = j_\mu(x_0, x_1, x_2) \delta(x_3),$$

$$\mu \in (0, 1, 2), \quad (20)$$

which allows us to do the k_3 integral in (19) analytically and obtain

$$D_{\mu\nu}(X-Y) = \int \frac{d^3K}{(2\pi)^3} e^{iK(X-Y)} \times \left[\frac{\delta_{\mu\nu}}{2\sqrt{K^2}} - (1-\xi) \frac{K_\mu K_\nu}{4\sqrt{K^2} K^2} \right]. \quad (21)$$

Note that in this equation the indices μ and ν are $\in (0, 1, 2)$, and therefore they should properly be written differently (as $\bar{\mu}$ and $\bar{\nu}$, for example), but to simplify the notation we use the same letters for these indices. We can rescale the gauge parameter $(1-\xi) \rightarrow 2(1-\bar{\xi})$ and suppress the bar to remove the factor of 1/4 in the last term in (21).

We introduce a three-dimensional vector field (which we again call A) and write the effective action

$$S = \int d^3X \left[\frac{1}{2} F_{\mu\nu} \frac{1}{\sqrt{-\partial^2}} F_{\mu\nu} + A_\mu J_\mu + \frac{1}{\xi} \partial \cdot A \frac{1}{\sqrt{-\partial^2}} \partial \cdot A \right], \quad (22)$$

which corresponds to (21) in the sense that if we integrate out the gauge field, we reproduce the dimensionally reduced propagator. We redefine the gauge-fixing term to be $(\partial \cdot A)^2/\xi$, add the kinetic term for the fermions [see Eq. (4)], and add a CS term to obtain

$$S = \int d^3X \left[\bar{\Psi} i \not{D} \Psi + \frac{1}{2} F_{\mu\nu} \frac{1}{\sqrt{-\partial^2}} F_{\mu\nu} + \frac{1}{2\xi} (\partial \cdot A)^2 + i\theta \epsilon_{\mu\nu\lambda} A_\mu \partial_\nu A_\lambda \right]. \quad (23)$$

We want to use this relativistic theory to describe graphene near the Dirac points. To do this, we replace the Euclidean metric in the first term of Eq. (23) with the noncovariant form

$$g_{\mu\nu} \rightarrow M_{\mu\nu} \text{ with } M = \begin{bmatrix} 1 & 0 & 0 \\ 0 & v_F & 0 \\ 0 & 0 & v_F \end{bmatrix}, \quad (24)$$

so that $\bar{\Psi} i \not{D} \Psi$ becomes $\bar{\Psi} i \gamma_\mu M_{\mu\nu} D_\nu \Psi$. We obtain the Feynman rules (in Landau gauge) from the resulting action:

$$S^{(0)}(p_0, \vec{p}) = -(i \gamma_\mu M_{\mu\nu} P_\nu)^{-1}, \quad (25)$$

$$G_{\mu\nu}^{(0)}(p_0, \vec{p}) = \left(\delta_{\mu\nu} - \frac{P_\mu P_\nu}{P^2} \right) \frac{1}{2\sqrt{P^2}}, \quad (26)$$

$$\Gamma_\mu^{(0)} = M_{\mu\nu} \gamma_\nu. \quad (27)$$

From this point on we will not refer again to the original four-dimensional theory. We define new notation so that lowercase letters denote the spatial components of three vectors [for example, $P = (p_0, \vec{p})$]. We also introduce some additional notational simplifications that will be used in the rest of this paper: we will sometimes write all momentum arguments of functions with a single letter [for example, $S(P) := S(p_0, \vec{p})$], we define $dK := dk_0 d^2k / (2\pi)^3$, and we write $Q = K - P$.

III. NONPERTURBATIVE THEORY

We will include nonperturbative effects by introducing fermion and photon dressing functions and solving a set of coupled Schwinger-Dyson (SD) equations.

A. Propagators and vertices

In the nonperturbative theory the bare propagator $S^{(0)}(P)$ in Eq. (25) is written with six dressing functions ($Z_P^+, A_P^+, B_P^+, Z_P^-, A_P^-, B_P^-$), where we have used subscripts instead of brackets to indicate the momentum dependence [for example, $Z_P^+ := Z^+(p_0, \vec{p})$]. We define two projection operators $\chi_\pm = \frac{1}{2}(1 \pm \gamma_3 \gamma_5)$. Using this notation, the fermion propagator has the form

$$S^{-1}(P) = [-i(Z_P^+ p_0 \gamma_0 \chi_+ + v_F A_P^+ \vec{p} \cdot \vec{\gamma}) + B_P^+] \chi_+ + [-i(Z_P^- p_0 \gamma_0 \chi_- + v_F A_P^- \vec{p} \cdot \vec{\gamma}) + B_P^-] \chi_-,$$

$$S(P) = \frac{1}{\text{Den}_P^+} [i(Z_P^+ p_0 \gamma_0 + v_F A_P^+ \vec{p} \cdot \vec{\gamma}) + B_P^+] \chi_+ + \frac{1}{\text{Den}_P^-} [i(Z_P^- p_0 \gamma_0 + v_F A_P^- \vec{p} \cdot \vec{\gamma}) + B_P^-] \chi_-,$$

$$\text{Den}_P^\pm = p_0^2 Z_P^{\pm 2} + p^2 v_F^2 A_P^{\pm 2} + B_P^{\pm 2}. \quad (28)$$

We define the even and odd functions:

$$X_\pm = X_{\text{even}} \pm X_{\text{odd}} \rightarrow X_{\text{even/odd}} = \frac{1}{2}(X_+ \pm X_-), \quad (29)$$

where $X \in (Z, A, B)$. In the notation of Sec. IIC, $B_{\text{even}}(0, 0)$ is a standard Dirac-type mass (denoted \mathcal{M}), which breaks chiral symmetry but not time-reversal symmetry, and $B_{\text{odd}}(0, 0)$ is a Haldane-type mass (\mathcal{M}^{35}), which preserves chiral symmetry but violates time-reversal invariance. In the bare theory $Z_\pm = A_\pm = 1$, and $B_\pm = 0$, and therefore the odd functions are zero. It is easy to see that (28) reduces to (25) in this limit.

The Feynman rule for the dressed vertex is

$$\Gamma_v(P, K) = \frac{1}{4}[H_{v\sigma}^+(P) + H_{v\sigma}^+(K)]\gamma_\sigma(1 + \gamma_5) + \frac{1}{4}[H_{v\sigma}^-(P) + H_{v\sigma}^-(K)]\gamma_\sigma(1 - \gamma_5), \quad (30)$$

where P is the outgoing fermion momentum, K is the incoming fermion momentum, and H^\pm indicates the diagonal 3×3 matrix

$$H^\pm(P) = \begin{bmatrix} Z^\pm(P) & 0 & 0 \\ 0 & v_F A^\pm(P) & 0 \\ 0 & 0 & v_F A^\pm(P) \end{bmatrix}. \quad (31)$$

It is clear that (30) and (31) reduce to (27) in the limit $Z_\pm = A_\pm = 1$. Equations (30) and (31) are the first term in the full Ball-Chiu vertex [19]. We include only the first term because calculations are much easier using this simpler ansatz and because in our previous calculation we found that the contribution of the additional terms is very small [20].

To define the dressed photon propagator we start with a complete set of 11 independent projection operators. Defining $n_\mu = \delta_{\mu 0} - q_0 Q_\mu / Q^2$, we write

$$\begin{aligned} P_{\mu\nu}^1 &= \delta_{\mu\nu} - \frac{Q_\mu Q_\nu}{Q^2}, & P_{\mu\nu}^2 &= \frac{Q_\mu Q_\nu}{Q^2}, & P_{\mu\nu}^3 &= \frac{n_\mu n_\nu}{n^2}, & P_{\mu\nu}^4 &= Q_\mu n_\nu, & P_{\mu\nu}^5 &= n_\mu Q_\nu, \\ P_{\mu\nu}^6 &= \epsilon_{\mu\nu\alpha} Q_\alpha, & P_{\mu\nu}^7 &= \epsilon_{\mu\nu\alpha} n_\alpha \frac{Q^2}{q^2}, & P_{\mu\nu}^8 &= \epsilon_{\mu\alpha\beta} Q_\alpha n_\beta Q_\nu, & P_{\mu\nu}^9 &= \epsilon_{\nu\alpha\beta} Q_\alpha n_\beta Q_\mu, \\ P_{\mu\nu}^{10} &= -\epsilon_{\mu\alpha\beta} Q_\alpha n_\beta n_\nu \frac{Q^2}{q^2}, & P_{\mu\nu}^{11} &= -\epsilon_{\nu\alpha\beta} Q_\alpha n_\beta n_\mu \frac{Q^2}{q^2}. \end{aligned} \quad (32)$$

Using this notation, the inverse dressed photon propagator can be written

$$G_{\mu\nu}^{-1} = 2\sqrt{Q^2} \left[P_{\mu\nu}^1 + \frac{1}{\xi} P_{\mu\nu}^2 \right] + 2\theta P_{\mu\nu}^6 + \Pi_{\mu\nu}, \quad (33)$$

where the polarization tensor is written in a completely general way as the sum

$$\Pi_{\mu\nu} = \sum_{i=1}^{11} a_i P_{\mu\nu}^i. \quad (34)$$

We invert the inverse propagator and then impose the constraints that the polarization tensor be transverse and satisfy the symmetry condition $\Pi_{\mu\nu}(Q) = \Pi_{\nu\mu}(-Q)$. The surviving components of the polarization tensor give

$$\Pi_{\mu\nu}(Q) = \alpha(Q) P_{\mu\nu}^1 + \gamma(Q) P_{\mu\nu}^3 + \Theta(Q) P_{\mu\nu}^6 + \rho(Q) [P_{\mu\nu}^{10} + P_{\mu\nu}^{11}], \quad (35)$$

and the propagator is

$$\begin{aligned} G_{\mu\nu} &= G_L P_{\mu\nu}^3 + G_T [P_{\mu\nu}^1 - P_{\mu\nu}^3] + G_D P_{\mu\nu}^6 + G_E [P_{\mu\nu}^{10} - P_{\mu\nu}^{11}], & G_L &= \frac{2\sqrt{Q^2} + \alpha}{(2\sqrt{Q^2} + \alpha)(2\sqrt{Q^2} + \alpha + \gamma) + Q^2(2\theta + \rho + \Theta)^2}, \\ G_T &= \frac{2\sqrt{Q^2} + \alpha + \gamma}{(2\sqrt{Q^2} + \alpha)(2\sqrt{Q^2} + \alpha + \gamma) + Q^2(2\theta + \rho + \Theta)^2}, \\ G_D &= -\frac{(2\theta + \Theta)(2\sqrt{Q^2} + \alpha + \gamma)}{(2\sqrt{Q^2} + \alpha)[(2\sqrt{Q^2} + \alpha)(2\sqrt{Q^2} + \alpha + \gamma) + Q^2(2\theta + \rho + \Theta)^2]}, \\ G_E &= \frac{(2\theta + \Theta)(2\sqrt{Q^2} + \alpha + \gamma) - (2\sqrt{Q^2} + \alpha)(2\theta + \rho + \Theta)}{(2\sqrt{Q^2} + \alpha)[(2\sqrt{Q^2} + \alpha)(2\sqrt{Q^2} + \alpha + \gamma) + Q^2(2\theta + \rho + \Theta)^2]}. \end{aligned} \quad (36)$$

B. Fermion Schwinger-Dyson equations

The inverse fermion propagator is written generically as

$$S^{-1}(P) = (S^{(0)})^{-1}(P) + \Sigma(P), \quad (37)$$

where the fermion self-energy is obtained from the SD equation as

$$\Sigma(P) = e^2 \int dK G_{\mu\nu}(Q) M_{\mu\tau} \gamma_\tau S(K) \Gamma_\nu. \quad (38)$$

Comparing (37) and (38) with (28), we find the operators that project out each of the fermion dressing functions. For example,

$$\mathcal{P}_{B^+} = \frac{1}{4}(1 + \gamma_5) \rightarrow B_p^+ = \text{Tr}[\mathcal{P}_{B^+} \Sigma(P)]. \quad (39)$$

Performing the traces, we obtain the set of self-consistent integrals that give the six fermion dressing functions:

$$\begin{aligned}
Z_P^\pm &= 1 - \frac{4\alpha\pi v_F}{2p_0} \int \frac{dK}{\text{Den}_K^\pm} \frac{q^2 G_L}{Q^2} k_0 Z_K^\pm (Z_K^\pm + Z_P^\pm), \\
A_P^\pm &= 1 + \frac{4\alpha\pi v_F}{2p^2} \int \frac{dK}{\text{Den}_K^\pm} \left\{ k_0 G_{DE}(\vec{q} \times \vec{p}) Z_K^\pm (A_K^\pm + A_P^\pm - Z_K^\pm - Z_P^\pm) \right. \\
&\quad + \frac{G_L}{Q^2} [q^2(\vec{k} \cdot \vec{p}) A_K^\pm (Z_K^\pm + Z_P^\pm) + k_0 q_0(\vec{p} \cdot \vec{q}) Z_K^\pm (A_K^\pm + A_P^\pm + Z_K^\pm + Z_P^\pm) \\
&\quad \left. - q_0(\vec{q} \times \vec{p}) B_K^\pm (A_K^\pm + A_P^\pm - Z_K^\pm - Z_P^\pm) \right\}, \\
B_P^\pm &= \frac{4\alpha\pi v_F}{2} \int \frac{dK}{\text{Den}_K^\pm} \frac{q^2 G_L}{Q^2} B_K^\pm (Z_K^\pm + Z_P^\pm). \tag{40}
\end{aligned}$$

We have used the notation $\vec{q} \times \vec{p} = q_1 p_2 - q_2 p_1$, $G_{DE} = G_D + G_E$ and dropped terms proportional to v_F^2 (relative to 1), which is the reason there are no terms containing factors G_T in (40).

From Eq. (40) it is easy to see that if we find a solution for the plus dressing functions Z^+ , A^+ , and B^+ , then we automatically have a solution for the minus dressing functions of the form $Z^- = Z^+$, $A^- = A^+$, and $B^- = -B^+$. We expect therefore that we will always be able to find a chirally symmetric and time-reversal-violating solution ($B_{\text{even}} = 0$ and $B_{\text{odd}} \neq 0$) if we initialize with $Z_{\text{odd}} = A_{\text{odd}} = B_{\text{even}} = 0$. We call this solution 1 and write the solutions for the nonzero dressing functions $Z_{\text{even}}^{(1)}$, $A_{\text{even}}^{(1)}$, and $B_{\text{odd}}^{(1)}$.

We can also see immediately that a solution with $Z_{\text{odd}} = A_{\text{odd}} = B_{\text{odd}} = 0$ should not exist since setting all odd dressing functions to zero on the right sides of Eqs. (40) gives $Z_{\text{odd}}(P) = B_{\text{odd}}(P) = 0$ but

$$\begin{aligned}
A_{\text{odd}}(P) &= \frac{4\alpha\pi v_F}{2p^2} \int \frac{dK}{Q^2} \frac{B_{K\text{even}}}{\text{Den}_{K\text{even}}} [q_0 G_L(\vec{q} \times \vec{p})(Z_{K\text{even}} + Z_{P\text{even}} - A_{K\text{even}} - A_{P\text{even}}) \\
&\quad + G_{DE} Q^2(\vec{p} \cdot \vec{q})(A_{K\text{even}} + A_{P\text{even}} + Z_{K\text{even}} + Z_{P\text{even}})]. \tag{41}
\end{aligned}$$

In the vicinity of the critical point, however, where $B_{K\text{even}}$ is small, we would have $A_{\text{odd}}(P) \approx 0$. We therefore expect to get rapid convergence if we start in the vicinity of the critical point and initialize with $Z_{\text{odd}} = A_{\text{odd}} = B_{\text{odd}} = 0$. We will call this solution 2.

We can also show that the two solutions discussed above are approximately the same, except for the reversal of the even and odd parts of the B dressing function. To see this we substitute on the right side of (40)

$$Z_{\text{odd}}^{(2)} = A_{\text{odd}}^{(2)} = B_{\text{odd}}^{(2)} = 0, \quad Z_{\text{even}}^{(2)} = Z_{\text{even}}^{(1)}, \quad A_{\text{even}}^{(2)} = A_{\text{even}}^{(1)}, \quad B_{\text{even}}^{(2)} = B_{\text{odd}}^{(1)}, \tag{42}$$

which gives

$$\begin{aligned}
Z_{\text{even}}^{(2)} &= Z_{\text{even}}^{(1)}, \quad B_{\text{even}}^{(2)} = B_{\text{odd}}^{(1)}, \quad A_{\text{even}}^{(2)} = A_{\text{even}}^{(1)} + \frac{4\alpha\pi v_F}{2p^2} \int \frac{B_{K\text{odd}}^{(1)}}{\text{Den}_K Q^2} \\
&\quad \times [q_0 G_L(\vec{q} \times \vec{p})(A_{K\text{even}}^{(1)} + A_{P\text{even}}^{(1)} - Z_{K\text{even}}^{(1)} - Z_{P\text{even}}^{(1)}) - G_{DE} Q^2(\vec{p} \times \vec{q})(A_{K\text{even}}^{(1)} + A_{P\text{even}}^{(1)} + Z_{K\text{even}}^{(1)} + Z_{P\text{even}}^{(1)})]. \tag{43}
\end{aligned}$$

The first two lines in (43) are consistent with (42), and the last line is approximately consistent when we are close to the critical point.

This analysis agrees with our numerical results, which are presented in detail in Sec. V. In summary, for all values of (α, θ) we have considered, we have found only two solutions, which have the form

$$\text{Solution 1: } Z_{\text{even}}^{(1)} \neq 0, \quad A_{\text{even}}^{(1)} \neq 0, \quad B_{\text{odd}}^{(1)} \neq 0; \quad Z_{\text{odd}}^{(1)} = A_{\text{odd}}^{(1)} = B_{\text{even}}^{(1)} = 0; \tag{44}$$

$$\text{Solution 2: } Z_{\text{even}}^{(2)} \approx Z_{\text{even}}^{(1)}, \quad A_{\text{even}}^{(2)} \approx A_{\text{even}}^{(1)}, \quad B_{\text{even}}^{(2)} \approx B_{\text{odd}}^{(1)}; \quad Z_{\text{odd}}^{(2)} \approx A_{\text{odd}}^{(2)} \approx B_{\text{odd}}^{(2)} \approx 0. \tag{45}$$

The approximately equal to symbols in the second line indicate deviations from zero of less than 0.01 percent. Solution 1 preserves chiral symmetry but violates time-reversal invariance, and to the degree of accuracy noted above, solution 2 breaks chiral symmetry but satisfies time-reversal invariance.

C. Photon Schwinger-Dyson equations

The two components of the polarization tensor denoted ρ and Θ can be set to zero in the approximation $v_F^2 \ll 1$, which is consistent with what was done with the fermion dressing functions in Sec. III B. In this case Eqs. (36) become

$$G_L = \frac{2Q + \alpha}{(2\sqrt{Q^2} + \alpha)(2\sqrt{Q^2} + \alpha + \gamma) + 4Q^2\theta^2}, \quad G_D + G_E \equiv G_{DE} = -\frac{2\theta}{(2\sqrt{Q^2} + \alpha)(2\sqrt{Q^2} + \alpha + \gamma) + 4Q^2\theta^2}. \tag{46}$$

TABLE II. Comparison of $B^+(0, 0)$ from different approximations for two different values of (α, θ) .

Approximation	$(\alpha, \theta) = (4.0, 0.2)$	$(\alpha, \theta) = (3.4, 0.6)$
(3,0,0)	0.00256085	0.00036157
(3,0,1)	0.00255782	0.00036102
(2,0,0)	0.00256082	0.00036167
(2,0,1)	0.00255762	0.00036080
(1,0,0)	0.00256083	0.00036168
(1,0,1)	0.00255762	0.00036080

These expressions involve only two components of the polarization tensor: $\alpha(p_0, p)$ and $\gamma(p_0, p)$. We work with the more convenient expressions

$$\Pi_{00} = \frac{q^2}{Q^2}(\alpha + \gamma), \quad (47)$$

$$\text{Tr}\Pi = \Pi_{\mu\mu} = \alpha + \frac{Q^2}{q^2}\Pi_{00}. \quad (48)$$

From the Schwinger-Dyson equation for the polarization tensor we obtain

$$\begin{aligned} \Pi_{00} = & -4\alpha\pi v_F \int \frac{dK}{\text{Den}_K^+ \text{Den}_Q^+} (Z_K^+ + Z_Q^+) \\ & \times [v_F^2(\vec{k} \cdot \vec{q})A_K^+ A_Q^+ + B_K^+ B_Q^+ - k_0 q_0 Z_K^+ Z_Q^+] \\ & + (+ \rightarrow -), \end{aligned} \quad (49)$$

where the notation $(+ \rightarrow -)$ indicates a second integral with the same form as the first but with all plus superscripts changed to minus. Similarly, we obtain for the trace

$$\begin{aligned} \Pi_{\mu\mu} = & -4\alpha\pi v_F \int \frac{dK}{\text{Den}_K^+ \text{Den}_Q^+} \{2v_F^2(A_K^+ + A_Q^+) \\ & \times (B_K^+ B_Q^+ + k_0 q_0 Z_K^+ Z_Q^+) + (Z_K^+ + Z_Q^+) \\ & \times [v_F^2(\vec{k} \cdot \vec{q})A_K^+ A_Q^+ + B_K^+ B_Q^+ - k_0 q_0 Z_K^+ Z_Q^+]\} \\ & + (+ \rightarrow -). \end{aligned} \quad (50)$$

Equations (40), (46), (49), and (50) form a complete set of self-consistent equations that involve only the approximation $v_F^2 \ll 1$.

Now we discuss some additional approximations for the photon propagator and dressing functions. From Eqs. (49)

and (50) it is straightforward to show that

$$\Pi_{\mu\mu} = \Pi_{00} + O(v_F^2), \quad (51)$$

and therefore to $O(v_F^2)$ we can set $\Pi_{\mu\mu} = \Pi_{00}$, which gives

$$\alpha(q_0, q) = -\frac{q_0^2}{q^2}\Pi_{00}. \quad (52)$$

From equation (52) we see that by making a Coulomb-like approximation we can set $\alpha(q_0, q) = 0$. The full Coulomb approximation involves setting $q_0 = 0$ everywhere in the photon propagator. We summarize as follows: For approximation 1

we use $(Z, A, B, \Pi)|_{v_F^2 \ll 1}$ and

$$\begin{aligned} G_L = & \frac{q^2 Q^2 \Pi_{00} - q^4 (\Pi_{\mu\mu} + 2Q)}{Q[Q^3 \Pi_{00}^2 - \Pi_{\mu\mu} q^2 (Q \Pi_{00} + 2q^2) - 4(1 + \theta^2) q^4 Q]}, \\ G_{DE} = & \frac{2\theta q^4}{Q[Q^3 \Pi_{00}^2 - \Pi_{\mu\mu} q^2 (Q \Pi_{00} + 2q^2) - 4(1 + \theta^2) q^4 Q]}. \end{aligned}$$

For approximation 2 we use $(Z, A, B, \Pi)|_{v_F^2 \ll 1}$ and $\Pi_{\mu\mu} = \Pi_{00}$ and

$$\begin{aligned} G_L = & \frac{q^2 q_0^2 \Pi_{00} - 2q^4 Q}{Q[q_0^2 Q \Pi_{00}^2 - 2q^4 \Pi_{00} - 4(1 + \theta^2) q^4 Q]}, \\ G_{DE} = & \frac{2\theta q^4}{Q[q_0^2 Q \Pi_{00}^2 - 2q^4 \Pi_{00} - 4(1 + \theta^2) q^4 Q]}. \end{aligned}$$

For approximation 3 we use $(Z, A, B)|_{v_F^2 \ll 1}$ and $\Pi|_{(v_F^2, q_0/q) \ll 1}$ and

$$\begin{aligned} G_L = & \frac{q^2}{Q[Q \Pi_{00} + 2(1 + \theta^2) q^2]}, \\ G_{DE} = & -\frac{\theta q^2}{Q^2[Q \Pi_{00} + 2(1 + \theta^2) q^2]}. \end{aligned}$$

For approximation 4, $(Z, A, B, \Pi)|_{v_F^2 \ll 1}$ $(G_L, G_{DE})|_{q_0=0}$,

$$\begin{aligned} G_L = & \frac{1}{\Pi_{00} + 2(1 + \theta^2) q^2}, \\ G_{DE} = & -\frac{\theta}{q[\Pi_{00} + 2(1 + \theta^2) q^2]}. \end{aligned}$$

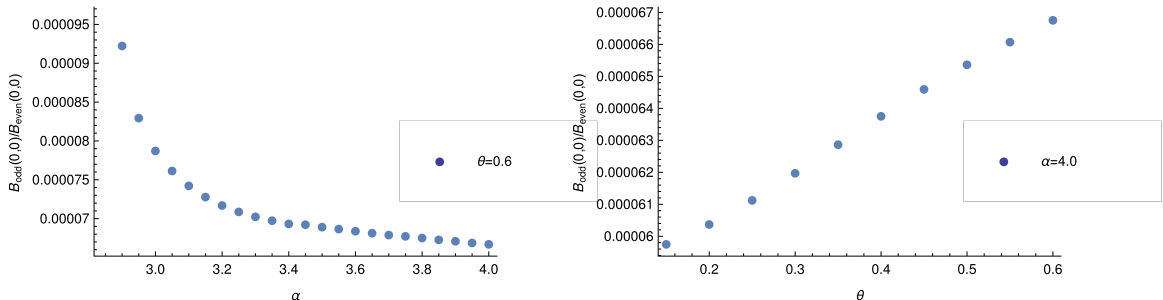


FIG. 1. The ratio of the odd mass divided by the even one for solution 2 [see Eq. (45)]. The left panel shows the ratio as a function of the coupling with $\theta = 0.6$, and the right panel shows the dependence on θ with $\alpha = 4.0$.

When $\theta = 0$ approximations 1 and 3 reduce to the full back-coupled calculation of Ref. [21], and approximation 4 reduces to the Coulomb version of that calculation.

We also consider using analytic results for the polarization components Π_{00} and $\Pi_{\mu\mu}$ obtained from the one-loop expressions using bare-fermion propagators. This is a commonly used approximation and is based on the vanishing fermion density of states at the Dirac points.

Finally, we note that although Eq. (46) indicates that G_{DE} is of the same order as G_L for values of θ of order 1, we expect that the contribution of this term to the fermion dressing functions will be small. To understand this point, recall that the propagator component G_T does not contribute in Eq. (40) because it drops out in the limit $v_F^2 \ll 1$. Likewise, in the second line of (40) the term proportional to G_{DE} is proportional to a difference of the form $Z - A$, and the first two lines of this equation show that this difference is of order v_F .

In summary, the full set of possible approximations we have discussed above can be written using the notation (n, m, l) , where (1) $n \in (1, 2, 3, 4)$ for approximation 1, 2, 3, or 4 [as defined following Eq. (52)], (2) $m \in (0, 1)$, where $m = 0$ means the polarization components Π_{00} and $\Pi_{\mu\mu}$ are obtained from their self-consistent expressions (back coupled) and $m = 1$ means we use their analytic one-loop approximations, and (3) $l \in (0, 1)$, where $l = 0$ means G_{DE} is set to zero and $l = 1$ means G_{DE} is included.

There are, in principle, 16 possible calculations, corresponding to approximations $n = (1, 2, 3, 4) \times m = (0, 1) \times l = (0, 1)$. Approximations $n \in (1, 2, 3)$ and $l \in (0, 1)$ agree to very high accuracy. We show some results for the values of $B^+(0, 0)$ which verify this in Table II. From this point on we will consider only approximations (3,0,0), (4,0,0), and (4,1,0).

IV. NUMERICAL METHOD

We need to solve numerically the set of eight coupled equations (40), (49), and (50) for the dressing functions Z^\pm , A^\pm , B^\pm , Π_{00} , and $\Pi_{\mu\mu}$. The functions Π_{00} and $\Pi_{\mu\mu}$ are renormalized by subtracting the zero-momentum value

$$\begin{aligned}\Pi_{00}^{\text{renorm}}(P) &= \Pi_{00}(P) - \Pi_{00}(0), \\ \Pi_{\mu\mu}^{\text{renorm}}(P) &= \Pi_{\mu\mu}(P) - \Pi_{\mu\mu}(0).\end{aligned}$$

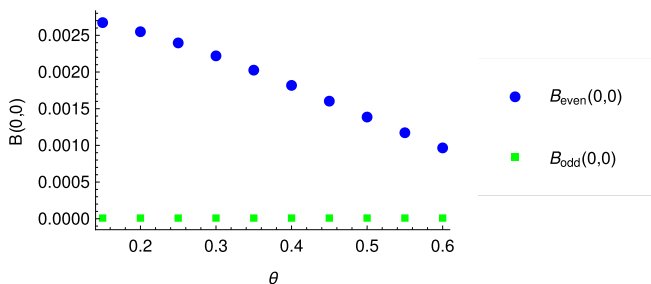


FIG. 2. $B_{\text{even}}(0, 0)$ and $B_{\text{odd}}(0, 0)$ as functions of the parameter θ with coupling $\alpha = 4.0$.

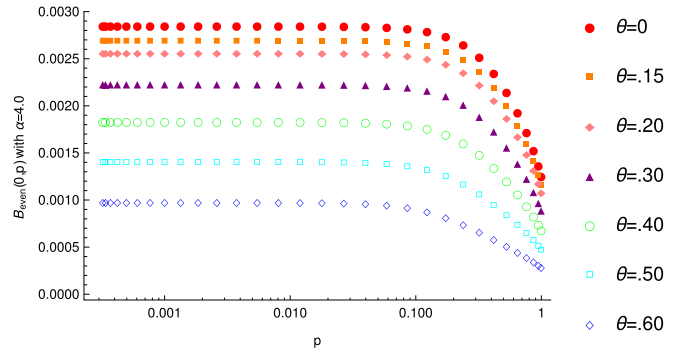


FIG. 3. $B_{\text{even}}(0, p)$ as a function of momentum at fixed $\alpha = 4.0$.

We work in spherical coordinates and define $\cos(\theta) = \vec{p} \cdot \vec{k}/(pk)$, so that the integrals have the form

$$\begin{aligned}\int dK &= \frac{1}{(2\pi)^3} \int_{-\infty}^{\infty} dk_0 \int_0^{\infty} dk k \int_0^{2\pi} d\theta f(k_0, k, \theta) \\ &= \frac{1}{(2\pi)^3} \int_0^{\infty} dk_0 \int_0^{\infty} dk k \int_0^{2\pi} \\ &\quad \times d\theta [f(k_0, k, \theta) + f(-k_0, k, \theta)].\end{aligned}\quad (53)$$

We use an ultraviolet cutoff Λ on all momentum integrals and define dimensionless variables $\hat{p}_0 = p_0/\Lambda$, $\hat{p} = p/\Lambda$, $\hat{k}_0 = k_0/\Lambda$, and $\hat{k} = k/\Lambda$. We also use generically $\hat{B} = B/\Lambda$ for all components and representations of the masslike fermion dressing function. The hatted momentum and frequency variables range from 10^{-6} to 1, and to simplify the notation we suppress all hats. We use a logarithmic grid in the k_0 and k dimensions to increase sensitivity to the infrared. We use Gauss-Legendre integration. Dressing functions are interpolated using double linear interpolation, using grids of $220 \times 200 \times 16$ points in the k_0 , k , and θ dimensions. In the calculation of $\Pi_{\mu\nu}$ we use an adaptive grid for the k_0 integral to more efficiently include the region of the integral where $k_0 \sim p_0$,

$$\int_{10^{-6}}^1 dk_0 = \int_{10^{-6}}^{p_0} dk_0 + \int_{p_0}^1 dk_0. \quad (54)$$

The integrands for the fermion dressing functions are smoother, and the adaptive grid is not needed.

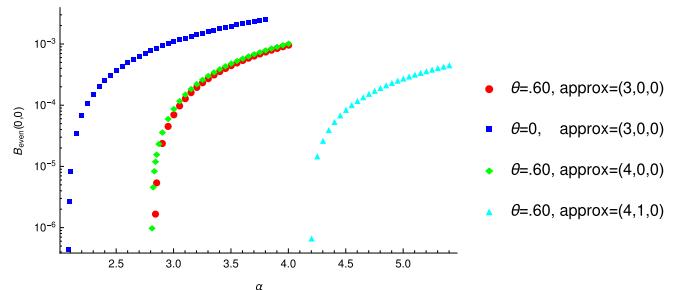


FIG. 4. $B_{\text{even}}(0, 0)$ as a function of coupling for different approximations and different values of the parameter θ .

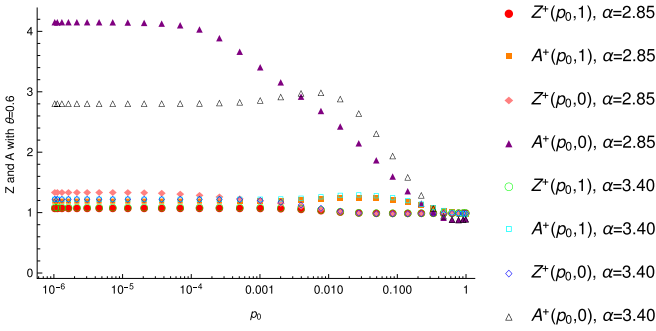


FIG. 5. The dressing functions Z^+ and Z^- as functions of p_0 , with p held fixed to its maximum and minimum values, for two values of α and $\theta = 0.6$.

V. RESULTS

Unless stated otherwise, all results in this section are obtained with the approximation (3,0,0).

In Refs. [20,21] we learned that using the Lindhard screening function, instead of calculating the photon polarization tensor using a self-consistently back-coupled formulation, produces an artificially large damping effect which increases the critical coupling. This result can be understood as arising from the fact that large fermion dressing functions Z and A are neglected in the denominator of the integral that gives the Lindhard expression for the polarization tensor. In this work we find that higher values of θ increase the critical coupling, and this result can be understood in the same way as resulting from increased screening.

We have found (for all values of θ and α considered) only two types of solutions [see Eqs. (44) and (45)]. Up to very small corrections, there is an odd mass solution (solution 1) and an even mass solution (solution 2), but no solutions for which both the even and odd mass parameters are nonzero. In Fig. 1 we show the absolute value of $B_{\text{odd}}(0, 0)/B_{\text{even}}(0, 0)$ for solution 2. As claimed following Eq. (45), this ratio is always less than 0.01%.

From this point on we show only results from solution 2. In Fig. 2 we show the condensates $B_{\text{even}}(0, 0)$ and $B_{\text{odd}}(0, 0)$ as a function of θ at fixed coupling, and in Fig. 3 we show the dressing function $B_{\text{even}}(p_0, p)$ as a function of momentum at fixed $p_0 = 0$, using different values of θ . Figures 2 and 3 show

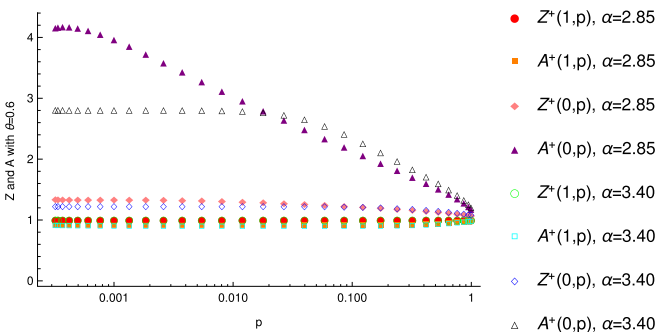


FIG. 6. The dressing functions Z^+ and A^+ as functions of p , with p_0 held fixed to its maximum and minimum values, for two values of α and $\theta = 0.6$.

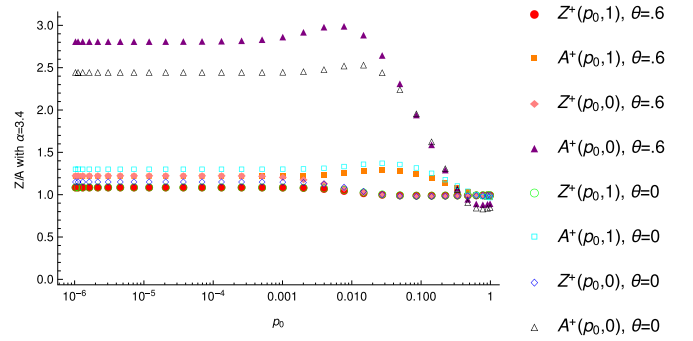


FIG. 7. The dressing functions Z^+ and A^+ as functions of p_0 for $\alpha = 3.4$ and $\theta \in (0, 0.6)$.

clearly that the condensate decreases as a function of θ , which implies that the critical coupling will increase as θ increases.

The dependence of the critical coupling on the parameter θ is seen explicitly in Fig. 4, which shows the condensate as a function of α for different values of θ , using different approximations.

In order to understand what drives this behavior, we look at the momentum dependence of the dressing functions Z and A . Figures 5 and 6 show the dressing functions Z^+ and A^+ as functions of p_0 and p with the other variable held fixed to its maximum or minimum value. The two values of α that are shown are $\alpha = 2.85$, which is close to the critical coupling for the value of $\theta = 0.6$ that is chosen, and $\alpha = 3.4$, which is relatively far from the critical coupling. One sees that the Z dressing function does not change much, but the A function does change and is responsible for the experimentally observed increase in the Fermi velocity at small frequencies as one approaches the critical coupling.

To see explicitly how this effect is influenced by the parameter θ , we show in Fig. 7 the fermion dressing functions Z^+ and A^+ as functions of p_0 for two different values of θ . Figure 7 shows that once again it is $A^+(p_0, 0)$ which changes the most and that the largest effect is obtained with the higher value of θ .

In Fig. 8 we show Π_{00} as a function of momentum for $\alpha = 3.4$ and two different values of θ . For comparison the Lindhard expression is also shown. Maximal screening is obtained with the Lindhard approximation, and the smallest

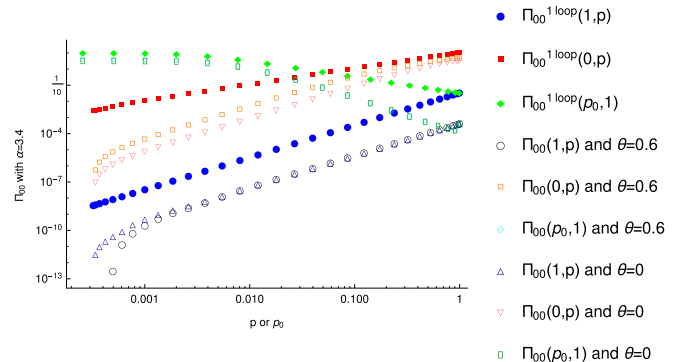


FIG. 8. The component Π_{00} as a function of p_0 and p for $\alpha = 3.4$ and $\theta \in (0, 0.6)$.

TABLE III. Extrapolated values of the critical coupling for different approximations and different values of the Chern-Simons parameter.

θ	Approximation		
	(3,0,0)	(4,0,0)	(4,1,0)
0.0	2.07	1.99	3.19
0.6	2.84	2.80	4.20

screening effect occurs when we set θ to zero. This is consistent with our results in Figs. 2 and 4, which show that the critical coupling increases with θ .

We fit the data shown in Fig. 4 using *Mathematica*, and the resulting function is extrapolated to obtain the value of the critical coupling for which $B_{\text{even}}(0, 0)$ goes to zero. Our results are collected in Table III. The result for approximation (4,1,0) with $\theta = 0$ is taken from [20], and the result for approximation (4,0,0) with $\theta = 0$ is taken from [21].

VI. CONCLUSIONS

Chern-Simons terms have been widely studied in condensed-matter physics in the context of chiral symmetry breaking, the Hall effect, and high-temperature superconductivity. In this work we showed that they are also relevant to the study of phase transitions in graphene. We worked with a low-energy effective theory that describes some features of monolayer suspended graphene. We used reduced QED₃₊₁, which describes planar electrons interacting with photons that can propagate in three spatial dimensions. We studied the effect of a Chern-Simons term in this theory. We found two classes of solutions: in the odd sector the theory dynamically generates a time-reversal-violating Haldane-type mass, and in the even sector a mass term of the standard Dirac type is generated. We studied the dependence of the Dirac mass on the Chern-Simons parameter θ and showed that it is suppressed as θ increases, which means that the critical coupling at which a nonzero Dirac condensate is generated increases with θ . We showed that this effect can be understood physically as arising from an increase in screening.

ACKNOWLEDGMENTS

This work was supported by the Natural Sciences and Engineering Research Council of Canada and the Helmholtz International Center for FAIR. The author thanks C. S. Fischer, L. von Smekal, and M. H. Thoma for hospitality at the Institut für Theoretische Physik, Justus-Liebig-Universität Giessen, and for discussions.

APPENDIX A: NOTATION

Our definitions of the lattice vectors are

$$\begin{aligned} a_1 &= a\{-\sqrt{3}, 0, 0\}, \\ a_2 &= \frac{a}{2}\{-\sqrt{3}, -3, 0\}, \\ a_3 &= \frac{a}{2}\{3\sqrt{3}, 3, 0\}. \end{aligned} \quad (\text{A1})$$

Using these definitions, the volume of the lattice cell is $S = \frac{3\sqrt{3}a^2}{2}$. The vectors that generate the positions of the nearest-neighbor lattice points are

$$\begin{aligned} \delta_1 &= \frac{a}{2}\{-\sqrt{3}, 1, 0\}, \\ \delta_2 &= \{0, -a, 0\}, \\ \delta_3 &= \{ \sqrt{3}, 1, 0\}, \end{aligned} \quad (\text{A2})$$

and the reciprocal lattice vectors are

$$\begin{aligned} b_1 &= \frac{2\pi}{a} \left\{ -\frac{1}{\sqrt{3}}, \frac{1}{3}, 0 \right\}, \\ b_2 &= \frac{2\pi}{a} \left\{ 0, -\frac{2}{3}, 0 \right\}, \\ b_3 &= \frac{2\pi}{a} \left\{ -\frac{1}{\sqrt{3}}, -\frac{1}{3}, 0 \right\}. \end{aligned} \quad (\text{A3})$$

The six K points are

$$K_i = \frac{3a}{2\pi} \begin{pmatrix} \frac{1}{\sqrt{3}} & 1 \\ \frac{4}{\sqrt{3}} & 0 \\ \frac{1}{\sqrt{3}} & -1 \\ -\frac{1}{\sqrt{3}} & -1 \\ -\frac{4}{\sqrt{3}} & 0 \\ -\frac{1}{\sqrt{3}} & 1 \end{pmatrix}, \quad (\text{A4})$$

and we choose our two inequivalent K points as

$$K_+ = -K_- = \left\{ -\frac{8\pi}{3\sqrt{3}a}, 0 \right\}. \quad (\text{A5})$$

We define the Fourier transform

$$\begin{aligned} a_{\vec{n}\sigma} &= \sqrt{S} \int_{\text{BZ}} \frac{d^2k}{(2\pi)^2} e^{i\vec{k}\cdot\vec{n}} a_\sigma(\vec{k}), \\ \sum_{\vec{n}} e^{i(\vec{k}-\vec{k}')\cdot\vec{n}} &= \frac{(2\pi)^2}{S} \delta^2(\vec{k}-\vec{k}'). \end{aligned} \quad (\text{A6})$$

Our representation of the γ matrices is

$$\begin{aligned} \gamma^0 &= \begin{pmatrix} 0 & 0 & 1 & 0 \\ 0 & 0 & 0 & 1 \\ 1 & 0 & 0 & 0 \\ 0 & 1 & 0 & 0 \end{pmatrix}, & \gamma^1 &= \begin{pmatrix} 0 & 0 & 0 & -1 \\ 0 & 0 & -1 & 0 \\ 0 & 1 & 0 & 0 \\ 1 & 0 & 0 & 0 \end{pmatrix}, \\ \gamma^2 &= \begin{pmatrix} 0 & 0 & 0 & i \\ 0 & 0 & -i & 0 \\ 0 & -i & 0 & 0 \\ i & 0 & 0 & 0 \end{pmatrix}, & \gamma^3 &= \begin{pmatrix} 0 & 0 & -1 & 0 \\ 0 & 0 & 0 & 1 \\ 1 & 0 & 0 & 0 \\ 0 & -1 & 0 & 0 \end{pmatrix}, \\ \gamma^5 &= \begin{pmatrix} 1 & 0 & 0 & 0 \\ 0 & 1 & 0 & 0 \\ 0 & 0 & -1 & 0 \\ 0 & 0 & 0 & -1 \end{pmatrix}. \end{aligned} \quad (\text{A7})$$

APPENDIX B: HALDANE-TYPE MASS

We consider a term in the Hamiltonian which would give counterclockwise hopping around the triangles that are

formed by each sublattice. We write

$$H_2 = t_2 \sum [i(a_{x_1}^\dagger a_{x_2} + a_{x_2}^\dagger a_{x_3} + a_{x_3}^\dagger a_{x_1})] \\ + t_2 \sum [i(b_{y_1}^\dagger b_{y_2} + b_{y_2}^\dagger b_{y_3} + b_{y_3}^\dagger b_{y_1})] + \text{H.c.}, \quad (\text{B1})$$

where $\{\vec{x}_1, \vec{x}_2, \vec{x}_3\}$ and $\{\vec{y}_1, \vec{y}_2, \vec{y}_3\}$ indicate the A and B sites on one hexagonal cell and the sums are over all A and B triangular sublattices. We will take the origin of the coordinate system to be at $\vec{x}_1 = (0, 0)$. Using our definitions of the lattice vectors, the corners of the triangular A and B sublattices which form the hexagon with \vec{x}_1 in the lower left corner are

$$\vec{x}_1 = (0, 0), \quad \vec{x}_2 = -\frac{\vec{a}_1}{\sqrt{3}} = a(1, 0), \\ \vec{x}_3 = -\frac{\vec{a}_2}{\sqrt{3}} = \frac{a}{2}(1, \sqrt{3}), \\ \vec{y}_1 = -\frac{2}{3}\vec{a}_1 + \frac{1}{3}\vec{a}_2 = \frac{a}{2\sqrt{3}}(\sqrt{3}, -1),$$

$$\vec{y}_2 = -\frac{2}{3}\vec{a}_1 - \frac{2}{3}\vec{a}_2 = \frac{a}{\sqrt{3}}(\sqrt{3}, 1), \\ \vec{y}_3 = -\frac{1}{3}\vec{a}_1 - \frac{2}{3}\vec{a}_2 = \frac{a}{\sqrt{3}}(0, 1). \quad (\text{B2})$$

Fourier transforming to momentum space and expanding around the Dirac points, we obtain

$$H_2 = t_2 \mathcal{C} \int \frac{d^2 p}{(2\pi)^2} \{ [a_+^\dagger(p) a_+(p) - a_-^\dagger(p) a_-(p)] \\ - [b_+^\dagger(p) b_+(p) - b_-^\dagger(p) b_-(p)] \} \\ = t_2 \mathcal{C} \int \frac{d^2 p}{(2\pi)^2} [\bar{\Psi}(p) \gamma^3 \gamma^5 \Psi(p)], \quad (\text{B3})$$

where we have defined the constant $\mathcal{C} = 2[\sin(2\phi) - 2\sin(\phi)]$, with $\phi = 8\pi/(3\sqrt{3})$. Equation (B3) shows that the Hamiltonian (B1) corresponds to a mass of the form \mathcal{M}^{35} in the effective theory.

-
- [1] R. D. Pisarski, *Phys. Rev D* **29**, 2423 (1984).
[2] T. W. Appelquist, M. Bowick, D. Karabali, and L. C. R. Wijewardhana, *Phys. Rev. D* **33**, 3704 (1986).
[3] A. Lopez and E. Fradkin, *Phys. Rev. B* **44**, 5246 (1991).
[4] V. P. Gusynin and P. K. Pyatkovskiy, *Phys. Rev. D* **94**, 125009 (2016).
[5] A. V. Kotikov and S. Teber, *Phys. Rev. D* **94**, 114011 (2016).
[6] T. Appelquist, M. J. Bowick, D. Karabali, and L. C. R. Wijewardhana, *Phys. Rev. D* **33**, 3774 (1986).
[7] T. Matsuyama and H. Nagahiro, *Mod. Phys. Lett. A* **15**, 2373 (2000); *Gravitation Cosmol.* **6**, 145 (2000).
[8] A. Bashir, A. Raya, and S. Sánchez-Madriral, *J. Phys. A* **41**, 505401 (2008).
[9] K. I. Kondo and P. Maris, *Phys. Rev. Lett.* **74**, 18 (1995); *Phys. Rev. D* **52**, 1212 (1995).
[10] A. P. Balachandran, E. Ercolessi, G. Morandi, and A. M. Srivastava, *Int. J. Mod. Phys. B* **04**, 2057 (1990).
[11] E. Witten, *La Rivista del Nuovo Cimento* **39**, 313 (2016).
[12] Y. Hosotani, *Phys. Lett. B* **319**, 332 (1993).
[13] I. A. Shovkovy, in *Strongly Interacting Matter in Magnetic Fields*, Lecture Notes in Physics Vol. 871 (Springer, Berlin, 2013), p. 13.
[14] F. D. M. Haldane, *Phys. Rev. Lett.* **61**, 2015 (1988).
[15] V. P. Gusynin, S. G. Sharapov, and J. P. Carabotte, *Int. J. Mod. Phys. B* **21**, 4611 (2007).
[16] E. C. Marino, *Nucl. Phys. B* **408**, 551 (1993).
[17] E. V. Gorbar, V. P. Gusynin, and V. A. Miransky, *Phys. Rev. D* **64**, 105028 (2001).
[18] E. V. Gorbar, V. P. Gusynin, V. A. Miransky, and I. A. Shovkovy, *Phys. Rev. B* **66**, 045108 (2002).
[19] J. S. Ball and T. W. Chiu, *Phys. Rev. D* **22**, 2542 (1980); **22**, 2550 (1980).
[20] M. E. Carrington, C. S. Fischer, L. von Smekal, and M. H. Thoma, *Phys. Rev. B* **94**, 125102 (2016).
[21] M. E. Carrington, C. S. Fischer, L. von Smekal, and M. H. Thoma, *Phys. Rev. B* **97**, 115411 (2018).